Fat tissue equivalent phantoms for microwave applications by reinforcing gelatin with nanocellulose

Biomedical Physics & Engineering Express

PAPER

Fat tissue equivalent phantoms for microwave applications by reinforcing gelatin with nanocellulose

Hana Dobšíček Trefná[1], Saül Llàcer Navarro[2,3], Fredrik Lorentzon[1,2], Tiina Nypelö[2,3] and Anna Ström[2]

[1] Signal Processing and Biomedical engineering, Department of Electrical Engineering, Chalmers University of Technology, Sweden
[2] Applied Chemistry, Department of Chemistry and Chemical Engineering, Chalmers University of Technology, Sweden
[3] Wallenberg Wood Science Center, Chalmers University of Technology, Sweden

E-mail: anna.strom@chalmers.se

Keywords: tissue-mimicking phantom, microwave diagnostics, hyperthermia, emulsion, gel, rheology

OPEN ACCESS

RECEIVED
1 July 2021

REVISED
28 August 2021

ACCEPTED FOR PUBLICATION
13 September 2021

PUBLISHED
7 October 2021

Abstract

Tissue mimicking phantom materials with thermal and dielectric equivalence are vital for the development of microwave diagnostics and treatment. The current phantoms representing fat tissue are challenged by mechanical integrity at relevant temperatures coupled with complex production protocols. We have employed two types of nanocellulose (cellulose nanocrystals and oxidized cellulose nanocrystals) as reinforcement in gelatin stabilized emulsions for mimicking fat tissue. The nanocellulose-gelatin stabilized emulsions were evaluated for their dielectric properties, the moduli-temperature dependence using small deformation rheology, stress-strain behavior using large deformation, and their compliance to quality assurance guidelines for superficial hyperthermia. All emulsions had low permittivity and conductivity within the lower microwave frequency band, accompanied by fat equivalent thermal properties. Small deformation rheology showed reduced temperature dependence of the moduli upon addition of nanocellulose, independent of type. The cellulose nanocrystals gelatin reinforced emulsion complied with the quality assurance guidelines. Hence, we demonstrate that the addition of cellulose nanocrystals to gelatin stabilized emulsions has the potential to be used as fat phantoms for the development of microwave diagnostics and treatment.

1. Introduction

Microwave applications for medical diagnostics and treatment are emerging in today's health care systems. Microwave devices have the advantages of being cost-effective, compact, and portable while providing fast acquisition. The high contrast between dielectric properties of healthy and malignant tissues compensate for mediocre spatial resolution so that the microwave systems can serve as a fast decision tool for diagnostics of stroke and traumas [1, 2], detection of breast cancer [3–6] or localization of epileptic brain activity [7]. Another application of microwaves is hyperthermia cancer treatment, in which the tumor temperature is elevated to therapeutic levels to kill the tumor cells and/or making them vulnerable to other treatment modalities, such as radiotherapy and chemotherapy [8–11].

Development and verification of both the diagnostic and treatment systems require tissue-mimicking phantoms. A phantom is a physical structure made from materials that together imitate the characteristics of the biological tissue in terms of either electromagnetic (EM) wave propagation, thermal redistribution of heat, or both. Microwave diagnostics is based on differentiating dielectric properties of tissue [12–16] and therefore demand phantoms that model the electrical conductivity and permittivity of the tissue with high accuracy. Hyperthermia phantoms have an additional demand of thermal equivalence to enable accurate measurements of power and temperature deposition patterns of the applicators [17, 18].

The phantoms are standardly divided into two classes, representing either high water content tissues, such as muscle, brain, or tumor, that have values of permittivity (ε_r) between 40–80 and electrical conductivity (σ) between 0.4–1 S m^{-1} [19] or the low water content tissues, such as fat or bone, that have values of ε_r between 6 and 25 and values of σ between 0.05–0.4 S m^{-1} in the frequency range of 100 MHz–1 GHz. Different compositions of phantoms mimicking muscle, brain, skin, and tumor have been proposed based on hydrophilic gel formers

such as agar-agar or carrageenan [20–23] polyacrylamide [24, 25], or gelatin [26–29]. In addition, the use of waste oil hardeners shows promise as a breast phantom via its ease of preparation, non-toxicity, and dielectric properties [30]. However, non-toxic, self-standing, easy to prepare, and thermally stable phantoms to represent the low water content tissues characterized by low ε_r are yet lacking. Numerous dry phantoms have been introduced in the past, their complicated preparation procedures and often poor reproducibility have hampered their use. Acetylene black mixed with aluminum powder and Laminac polyester resin [31], carbon-doped paraffin solution dispersed in silicone rubber [32], and graphite powder and urethane rubber [33] are examples of currently available phantoms. Alternative to solid or semi-solid phantoms is the use of water dispersions of glycerin or nonionic surfactant Triton-X to tune permittivity for complex breast phantoms [34]. The liquids are poured into 3D printed containers derived from magnetic resonance imaging. However, often the thermal equivalence required for hyperthermia is not met, and the phantoms are neither self-standing nor cuttable, and the plastic containers can distract the EM field propagation on the boundary between the liquid and plastic, thus challenging the diagnostics [35].

The oil-in-water emulsion phantom that utilizes gelatin as a solidifier of a matrix that encloses the oil droplets in the structure that are responsible for providing the dielectric properties in the range of fat tissue, has the potential to overcome such challenges [26, 27, 29]. Gelatin forms a random coil conformation in hot water, upon cooling, it forms a self-standing gel through the formation of rigid triple helices connected by flexible links [36, 37]. The shear modulus and the strength of the resulting gel are defined by the concentration of triple helices [37]. Gelatin is used in a vast range of applications from food to pharma [38] and is hence readily available. The temperature at which the solution to gel (sol-gel) transition occurs is typically between 25 –35 °C, and it is independent of gelatin concentration [39, 40]. The sol-gel transition of gelatin is reversible, albeit with hysteresis [41]. Di Meo and co-workers [29] advanced previous gelatin emulsion protocols, preparing a non-toxic, easy-to-prepare sunflower—gelatin emulsion. Their gelatin emulsion showed good reproducibility and storage possibilities of at least ten days. In addition, they show that values of ε_r for the gelatin—sunflower emulsions can be adjusted as a function of oil content according to the Bruggeman formulation for up to 68 wt% oil. Despite promising properties for use in microwave diagnostics phantoms [27, 28], the thermal stability of the latest has not been reported.

Cellulose materials are widely used in engineered and pharmaceutical products such as paper and tablets. The establishment of cellulose nanomaterials has furthermore expanded the use of cellulose as viscosity modifier and to reinforce composite materials [42]. Cellulose particles have been demonstrated to provide strength to gelatin networks [43]. Of specific interest have been the nanosized cellulose particles that can be dispersed in a hydrophilic environment such as water [44]. Further surface modification of the nanosized celluloses has been shown to enable a chemical linkage between gelatin and the cellulose, creating covalent reinforcement of the network. The specifically demonstrated modification has involved oxidation of cellulose hydroxyl groups into carbonyl groups that can form a covalent imine bond with amine groups of lysine in gelatin [45, 46].

In this work, we have utilized emulsions kinetically stabilized by gelatin and nanocellulose to prepare self-standing phantoms with the dielectric and thermal properties of low water content tissues. Three different phantoms were developed; emulsions stabilized by gelatin, emulsion stabilized by gelatin and cellulose nanocrystals (CNC), and emulsion stabilized by gelatin and dialdehyde CNC, hereafter referred to as DAC. We have demonstrated that all developed fat-mimicking phantoms fulfill requirements of dielectric and mechanical properties. In addition, the nanocellulose reinforced the thermal integrity of the phantoms, increasing the temperature range at which the phantom can be used.

2. Material and methods

2.1. Materials

CNCs were purchased from Celluforce (Canada). Gelatin was kindly provided by Gelita, Sweden, Bloom 296 Gelatin A. Solec lecithin B-10 was kindly provided by Dupont, Denmark. Sodium periodate and hydroxylamine were purchased from Merck, Sweden. Rapeseed oil was a commercial grade purchased from a local supermarket (Coop X-tra brand), Sweden. Milli-Q water was used throughout the study with the resistivity of 18.2 Ω^{-1} cm^{-1} at 25 °C.

2.2. Methods

2.2.1. CNC dispersion

CNCs were dispersed in Milli-Q water at 3.5 wt% concentration. The dispersion was mixed with a magnetic stirrer during the addition of CNCs into water, followed by horizontal shaking at room temperature overnight. The dispersion was ultrasonicated for 15 min (VWR USC900D), ensuring that the temperature did not increase above 40 °C.

2.2.2. Production of dialdehyde CNCs through oxidation (DAC)

The oxidation of CNCs was performed according to Dash, Foston [46] using a weight ratio of sodium periodate to CNC of 0.7. The reaction time was 6 h, and the reaction vessel was covered with aluminum foil. The reaction was quenched by the addition of glycerol, after which it was dialyzed in water for two days using membranes with 12–14 000 g mol^{-1} cutoff.

Table 1. Final compositions of the gelatin and CNC/DAC-gelatin stabilized emulsions. All concentrations are given in wt%, based on the total weight of the final emulsion.

Sample name	Water	Oil	Lecithin	Gelatin	CNC	DAC
Gelatin stabilized emulsion	27.4	70	0.6	2	—	—
CNC-gelatin stabilized emulsion	26.8	70	0.6	2	0.6	—
DAC-gelatin stabilized emulsion	26.8	70	0.6	2	—	0.6

The solid content of the dialyzed dispersion was 3 wt%. The dispersion was stored at 4 °C until further use.

2.2.3. Preparation of gelatin stabilized emulsions

The oil and water were heated separately to 60 °C. Lecithin was dispersed in the hot water and left to mix for 10 min, after which the gelatin was let to dissolve for 20 min. Oil was then added dropwise to the gelatin-water system under vigorous stirring using Ultra-turrax (IKA T50), resulting in a visually turbid system. The system was poured into molds and cooled to 20 °C. The size of the molds used for preparing emulsions for mechanical testing was 10 mm in diameter and height, and for analysis of dielectric properties 100 mm in diameter. The emulsions were kept refrigerated until further use. See table 1 for the final compositions of emulsions used in this study.

2.2.4. Preparation of CNC/DAC-gelatin stabilized emulsions

The emulsions were prepared similar to the gelatin emulsions except that the CNC or DAC dispersions were heated to 50 °C, added to the gelatin-water system, and further incorporated with the oil. Note that the gelatin solution has to be of a high concentration as the system is diluted by the water dispersion of CNC and DAC. See table 1 for the final compositions of emulsions used in this study.

Confocal laser scanning microscopy (CLSM) was used for visualization of the emulsion structure using the Nikon Ti-E/A1 + microscope.

2.2.5. Differential scanning calorimetry (DSC)

Heat capacities were determined using Mettler-Toledo, model DSC 2. STARe software was used for calculating the specific heat using the average of the range of 15 °C to 45 °C in a heating ramp of 1 K min^{-1}. Medium pressure crucibles of 7 mm diameter (ME-29990) were used.

2.2.6. Rheology

The rheological properties of the emulsions were determined using a DHR-3 rheometer from TA Instruments, Denmark. The geometry used was plate-plate (40 mm in diameter) with a gap of 1 mm. The upper plate was equipped with a solvent trap and used with a custom-made evaporation chamber from TA Instruments. The samples were added to the plate at 60 °C, the upper plate was lowered to measurement position, and the temperature was reduced to 10 °C with a rate of 2 °C min^{-1}. The storage (G′) and loss (G″) modulus of the samples were recorded at a frequency of 1 Hz and a strain of 0.5%. The temperature was controlled with a Peltier plate.

2.2.7. Dielectric properties

The dielectric properties were measured by an open-ended coaxial dielectric probe (Dielectric Probe Kit DAK 12 (SPEAG, Switzerland) connected to a vector network analyzer (VNA) (Keysight FieldFox, Keysight, USA). The application operation frequency range is 10 MHz to 3 GHz with sweep of 101 points. The dielectric properties of each sample were measured twice at five different locations and are given as an average of all, typically 10 replications.

2.2.8. Mechanical properties

Mechanical properties of the gels were determined using a texture analyzer TA-HDi from Stable Micro-systems, UK. The tests were carried out at room temperature. Gels for stress-strain testing were prepared by pouring the hot dispersion into molds of 10 mm in diameter and 10 mm in height. Stress-strain curves were determined at a crosshead speed of 2 mm s^{-1}. The crosshead had a diameter of 20 mm. Free expansion of the gels was assured in the radial direction. True stress (σ_t) and true strain (ε_t) were calculated using equations (1) and (2):

$$\sigma_t = \frac{F\left(\frac{L}{L_0}\right)}{A_0} \tag{1}$$

$$\varepsilon_t = \log\left(\frac{L}{L_0}\right) \tag{2}$$

Where L and L_0 are the height and the initial height of the gels, respectively, A_0 is the initial cross-section area, and F is the force.

2.2.9. Testing for compliance with QA guidelines for superficial hyperthermia

Figure 1 shows a schematic representation and a photograph of the setup used for evaluation of the performance of fat phantoms during the hyperthermia QA procedure. The composition follows the QA applicator verification arrangement for superficial hyperthermia as described in [17, 18].

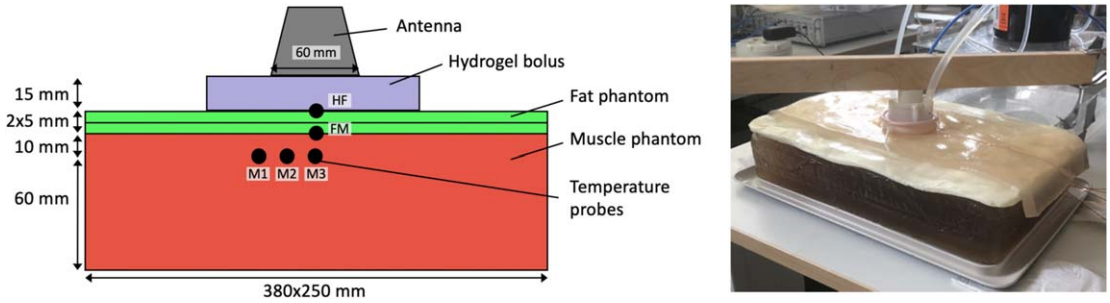

Figure 1. Schematic illustration (to the left) and photograph of the hyperthermia QA procedure (to the right). The different parts used, their dimensions, and the location of temperature probes are shown in the illustration.

In the arrangement (figure 1), a self-grounded antenna [47] was centered on top of a 15 mm thick hydrogel bolus [48] placed on top of the multilayered phantom. The applicator has a surface area with a diameter of 60 mm, and water temperature inside the enclosure was kept constant at 20 °C by circulation. The reflection coefficient of the antenna at frequency 485 MHz was −14.7 dB. The power of 60–63 W was applied for 6 min. The hydrogel bolus [48] was used to ensure both an optimal contact area with the phantom and extension beyond the radiating aperture. The hydrogel bolus ($400 \times 210 \times 15 mm^3$) was placed on top of the multilayered phantom consisting of a 70 mm high muscle-equivalent phantom, upon which two 5 mm fat phantoms of the same area as the muscle phantom were placed. The muscle phantom ($380 \times 250 \times 70\ mm^3$) was composed of water, sugar, salt, and agarose [20]. The ε_r of the muscle phantom and hydrogel bolus was 59.2 and 81, respectively. The σ for the muscle phantom and the hydrogel bolus was 0.71 S m^{-1} and 0.12 S m^{-1}, respectively. The phantom and bolus were at room temperature at the start of the experiments, and their temperatures were not regulated during the heating.

The temperature during the experiments was captured by fiber optic probes (THR-NS-882X, FISO Technologies Inc, Canada) located at three different depths in the center of the central plane of the antenna: at the interface between (a) bolus and fat phantom (HF), (b) fat and muscle phantom (FM), (c) at 1 cm depth in the muscle phantom (M1–M3). The three probes located in the muscle phantom contained multiple sensors spaced 10 mm from each other. The temperature distribution in the horizontal plane at the top layer of the fat phantom was captured by an infrared camera (B355, FLIR Systems, USA).

3. Results

3.1. Dielectric properties and heat capacity

Prediction of dielectric properties of mixtures is complex [49] following modified mixing rule principles. Figure 2(a) illustrates the prediction of permittivity as a function of oil content. Maxwell-Garnett effective medium approximation is valid at low volume fractions of oil, assuming that the domains are spatially, and via interactions, separated [50]. Bruggeman approximation excludes the effect of symmetry via volume fraction utilization, however, it has limitations above the percolation threshold. The semi-empirical Lichtenecker's logarithmic mixture formula, which has proven to be a useful practical formulation for determining the effective permittivity of homogenized dielectric mixtures [51], provides a similar prediction of permittivity at high oil fractions as Bruggeman. Thus, Maxwell-Garnett and Lichtenecker approximations act as a lower and upper bound for the permittivity establishment, indicating 0.7 being the lowest oil fraction required to reach low permittivities ($\varepsilon_r < 15$). We have therefore focused this study on compositions with the oil concentration of 70%. The compositions used (table 1) led to structures where the oil is enclosed in droplets in the gelatin matrix (figure 2(b)). The inherent instability of emulsions where the oil droplets coalesce, and phase separate, is here restricted by the gelatin matrix. The gelatin network will kinetically trap the oil droplets and hinder them from growing and ultimately separate from the matrix.

The dielectric properties over the frequency range of 0.1–3 GHz of the emulsions presented in table 1 represent the mean values with the confidence interval from measurements at 5 different locations (figure 3). All emulsions exhibited permittivities of ∼7–14.5. In addition, they exhibit low conductivities, hence complying with the dielectric requirements of a fat phantom. The gelatin stabilized emulsion is of the highest permittivity with values decreasing from ∼14.5 at 10 MHz to above 12 at 3 GHz. The CNC-gelatin reinforced phantom exhibited permittivity between 7 and 9. The permittivity values obtained lay within the bounds of Maxwell-Garnett and Lichtenecker. The specific heat of the emulsions was C_p 3218 J $(kg\ K)^{-1}$.

3.2. Rheological and mechanical properties

Shear rheology was used to determine absolute moduli at T = 20 and 45 °C, as well as the temperatures at which the gels set and melt. The rheological behavior

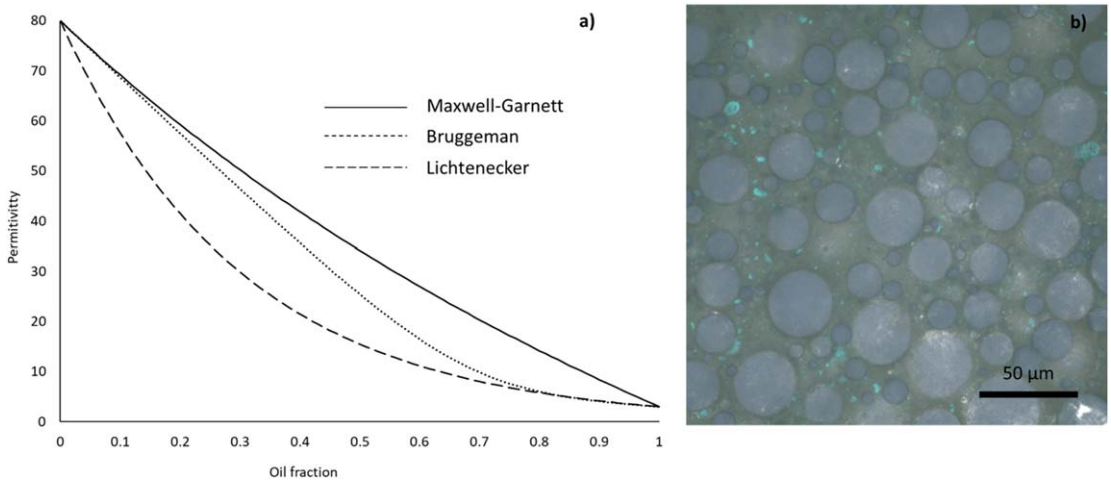

Figure 2. Prediction of emulsion permittivity as a function of oil fraction according to Maxwell-Garnett, Bruggeman, and Lichtenecker approximations (a) and CLSM visualization of a 70/30 gelatin stabilized oil emulsion where oil droplets are enclosed in gelatin matrix (b).

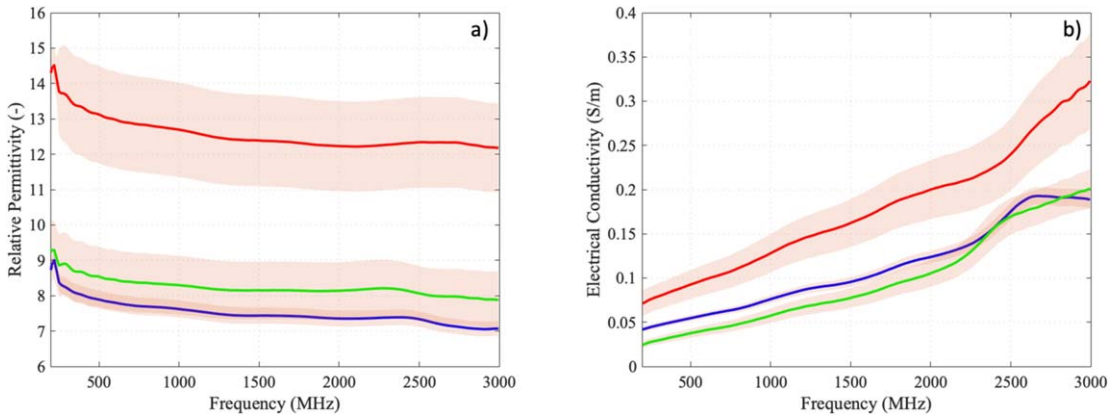

Figure 3. Permittivity (a) and conductivity (b) of the gelatin (red), CNC-gelatin (blue), and DAC-gelatin (green) stabilized emulsions.

at T = 20 °C is important given it is close to typical room temperature, and T = 45 °C as this is a temperature that a fat phantom should support without loss in mechanical integrity. Figure 4 shows that all emulsions exhibit three phases, one phase where the G′ is high, which occurs at temperatures close to room temperature or below (green shade in figure 4), a second phase where moduli are reduced rapidly (orange shade, figure 4) and the third one occurring at T > 40 °C (pink shade, figure 4). The gelatin stabilized emulsion shows a temperature behavior typical for pure gelatin where the gel sets (G′ > G″) at T = 30 °C (arrow 1 in figure 4(a)), followed by a sharp increase in G′ until T = 10 °C. As the gelatin stabilizing emulsion is reheated, we observe a plateau and sharp reduction in G′ at approximately T = 25 °C. The crossover G′ > G″, defined as the melting temperature, appears at approximately 38 °C (arrow 2 in figure 4(a)), after which the emulsion is dominated by the viscous component and behaves as a liquid (pink shaded area).

The moduli of the CNC-gelatin (figure 4(b)) and the DAC- gelatin (figure 4(c)) stabilized emulsions behave similarly upon reduction and increase in temperature. There is no clear setting or melting transition in neither gel, hence the absence of arrows 1 and 2 in figures 4(b) and (c). Instead, G′ remains at 80–100 Pa within the temperature range of 40 to 60 °C (red shaded area in figures 4(b) and (c)) and 2000 and 3000 Pa respectively within the temperature range of 10 and 25 °C (green shaded area in figures 4(b) and (c)). It is still possible to observe the sharp increase and decrease in the moduli, similar to gelatin stabilized emulsion, with the difference that moduli are not reduced to the same extent at the higher temperatures, and the materials still exhibit G′ > G″, thus are dominated by the elastic component.

The force exerted on the fat phantom during use is uniaxial compression. Therefore, the stress-strain response of the systems was tested. The stress at break and strain at break are shown in figure 5. We can see (figure 5(a)) that the stress at break for

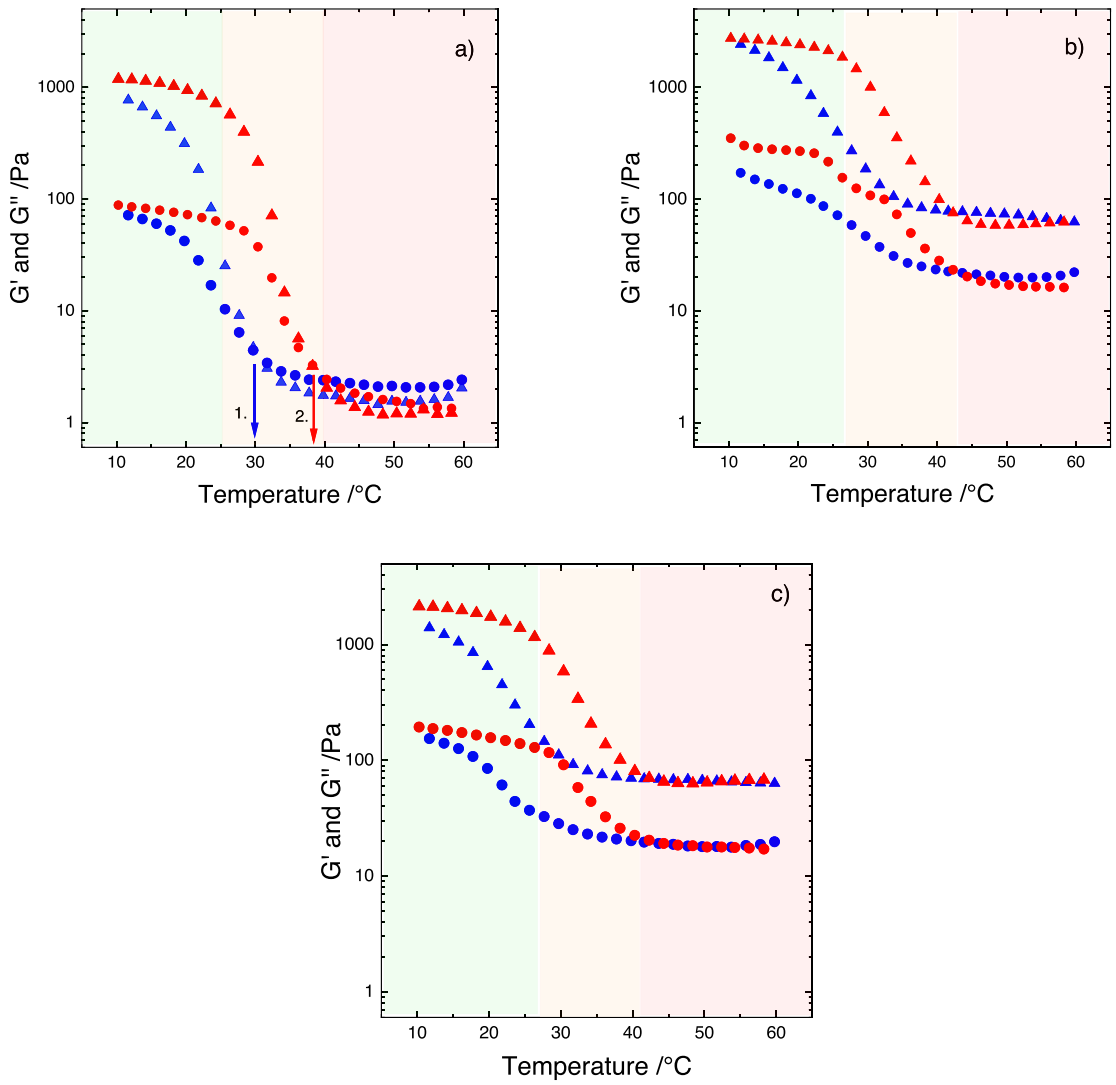

Figure 4. G′ (triangles) and G″ (circles) moduli as a function of temperature for (a) gelatin (b) CNC-gelatin (c) and DAC-gelatin stabilized emulsion. The samples were added at 60 °C, followed by cooling (blue symbols) and heating (red symbols). Arrow 1 and 2 points at the setting and melting temperatures of the gel. The measurements were performed at f = 1 Hz and strain 0.5%.

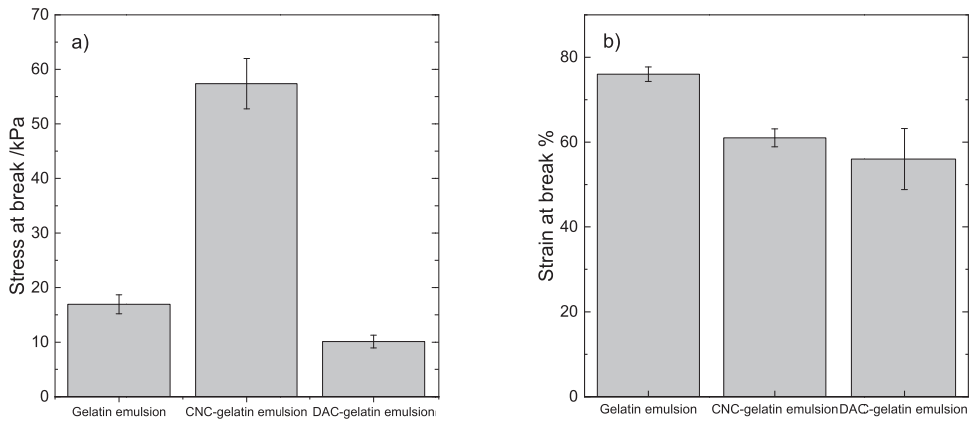

Figure 5. Stress at break (a) and strain at break (b) at room temperature for the gelatin, CNC-gelatin and DAC-gelatin stabilized emulsions.

the CNC-gelatin stabilized emulsion is the highest (approx. 57 kPa), followed by gelatin stabilized emulsion (approx. 18 kPa) and DAC-gelatin stabilized emulsion (approx. 10 kPa). The strain at which the gelatin emulsion broke was 75%, while CNC broke at 60% and DAC at approx. 58% (figure 5(b)).

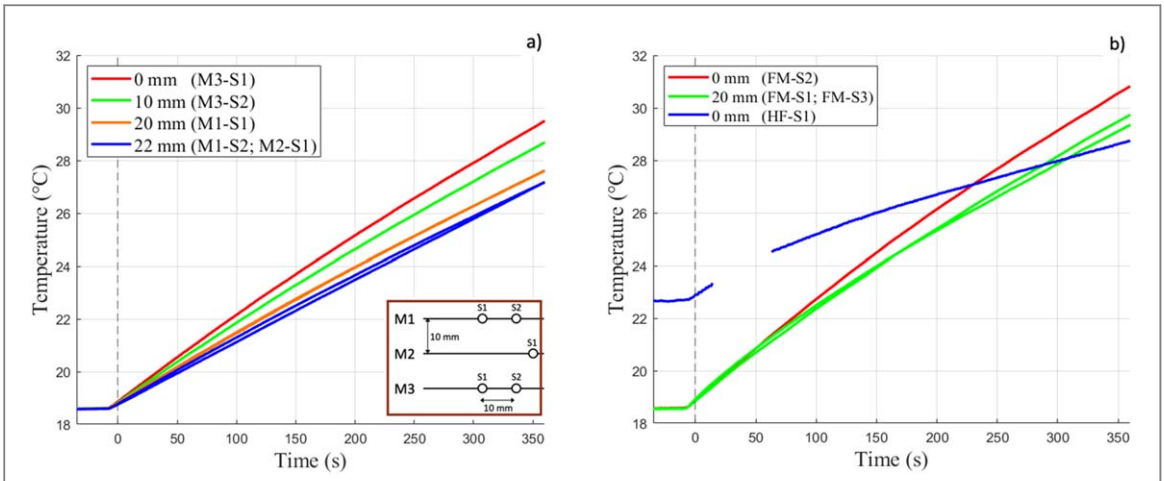

Figure 6. Temperatures at different positions (a) in the horizontal plane of the muscle phantom and (b) at boundaries between muscle/fat and fat/hydrogel bolus (for labeling see figure 1).

3.3. Phantom validation: the compliance with QA guidelines for superficial hyperthermia

The phantoms were exposed to microwave radiation (60–63 W) from a single antenna for 6 min in a setup presented in figure 1, and temperature was monitored at different locations by thermal sensors. Figure 6(a) shows the temperature at different locations in a horizontal plane, one centimeter below the muscle phantom surface. The antenna was centered above sensor 8 in the probe M3 and temperature rise in the other probes is given with respect to the distance of the probe to the center. The temperature increased by nearly 11 °C during the 6 min test confirming an appropriate function of the antenna and correct execution of the experimental validation.

The temperature at the boundaries between the muscle and fat phantoms and between fat and bolus (figure 6(b)) are relevant for the fat phantom verification. The highest temperature of approx. 31 °C was measured at the muscle-fat boundary right below the antenna center, with the temperature being approximately 1 °C lower, 2 cm from the center (measured at two positions, FM-S1 and FM-S3). The temperature between the bolus and antenna boundary was measured at a distance of approximately 1 cm from the central plane due to slight dislocation of the temperature sensor. The temperature between the bolus and antenna reaches a plateau more rapidly than the temperature at the fat-muscle boundary, this is related to the antenna cooling.

The temperature distributions captured by IR camera immediately after removal of the antenna and hydrogel bolus indicate that the maximal temperatures achieved at the top of the phantom ranged between 34 –36 °C for gelatin and DAC reinforced phantom while 30 °C for the CNC reinforced phantom (figures 7(a)–(c)). The deviation in the heating rates can be attributed to divergence in phantom conductivities. It is apparent that the pure gelatin phantom failed to withstand the stress exerted by the antenna in combination with temperature increase (figure 7(d)). As visible in figure 7(f), the DAC reinforced phantom showed damages at several locations, owing to the physical handling of the phantom.

4. Discussion

In this work, we hypothesized that the addition of CNCs within the gelatin network could increase its melting temperature, one of the major limitations in the use of gelatin reinforced phantoms. Indeed, the influence of temperature on the moduli of the gelatin stabilized emulsion shows distinct sol-gel transition at 28 °C upon cooling and gel to sol upon heating, at 38 °C (figure 4(a)). The emulsion stabilized only by gelatin can thus be defined as a liquid at $T > 38$ °C, making an application as fat phantom according to hyperthermia QA procedures challenging.

While the CNC and DAC stabilized emulsions weaken and the difference between G' and G'' is reduced, at $T > 28$ °C, the weakening is not to the same extent as the gelatin stabilized emulsion, and importantly, they do not exhibit gel-sol transition at 38 °C. The reduced temperature dependence for these systems can be explained through two different routes. In the case of CNC addition, we believe that we have an electrostatic attraction between the negatively charged CNC and the positively charged gelatin. In the case of the addition of DACs in the gelatin matrix, we have an electrostatic attraction like the CNC-gelatin matrix but also a covalent linkage between the aldehyde of the DAC and the amine on the gelatin. Thus, both CNC and DAC addition to gelatin provide increased thermal stability within the investigated temperature range. The results found for DAC gelatin interaction correspond to those reported by Dash and co-workers, [46].

The QA testing of the different emulsions clearly shows that gelatin stabilized emulsion cannot be used as a fat phantom, owing to large damages of the

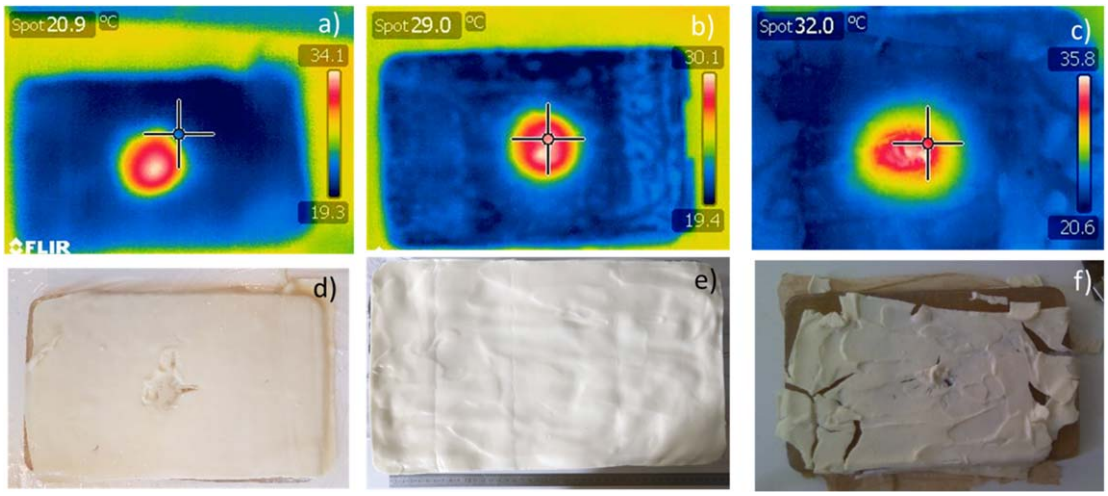

Figure 7. Heat distribution of the top layer as captured by IR camera (a), (b), and (c) and visual appearance (d), (e), and (f) after QA validation for superficial hyperthermia of gelatin reinforced fat phantom (a) and (d), CNC-gelatin reinforced fat phantom (b) and (e), and DAC-gelatin reinforced fat phantom (c) and (f).

Table 2. Consideration of gelatin, CNC-gelatin, and DAC-gelatin reinforced phantom suitability for hyperthermia QA procedures. The attributes are rated as achieved (+) or not achieved (−) based on the experimental work in this study.

	Gelatin reinforced phantom	CNC-gelatin reinforced phantom	DAC-gelatin reinforced phantom
Commercial availability of ingredients	+	+	—
Phantom can be prepared at a clinic with a heating plate and high-speed mixing	+	+	—
Dielectric properties are equivalent to fat tissue	+	+	+
Thermal stability	—	+	+
Proof of concept demonstration	—	+	—

phantom under the conditions (power, dielectric properties, and time of exposure) used here. The IR image of the gelatin reinforced phantom shows that the temperature reaches those temperatures within the area of rapid reduction of gel strength (orange shade figure 4(a)). The CNC-gelatin and DAC-gelatin reinforced phantom maintained physical integrity throughout the same heating procedure, confirming the increased thermal stability obtained through the addition of CNC and DAC, in agreement with rheological data.

The surface of the fat phantom is smooth for the gelatin (figure 7(a)) while more uneven for the CNC-gelatin and DAC- gelatin reinforced phantoms (figures 7(e) and (f)). This is related to the fact that gelatin behaves as a liquid at the temperatures at which the top layer is prepared, thus easily being poured into the mold. Instead, the CNC-gelatin and DAC-gelatin stabilized emulsions are gel-like (figures 4(b) and (c)) at similar temperatures, thus not filling the mold as efficiently as the gelatin stabilized emulsion.

The stress at break of the DAC-gelatin stabilized emulsion is lower than that of the CNC-gelatin stabilized emulsion (figure 5), which explains the larger amount of damages shown by the DAC-gelatin reinforced phantom during the QA test (figure 7(f)).

Table 2 summarizes the different aspects considered during the testing of the three proposed phantoms. The successful QA verification of the CNC-gelatin stabilized emulsion, in combination with the dielectric properties matching those of fat tissues, shows its potential for use as a fat phantom.

Subject to further studies is the behavior of the CNC-gelatin reinforced phantom under higher heating rates than used here (2 °C min^{-1}), as this may be required in some applications. In addition, the physical networks are subject to relaxations under stress [52] and may yield and reform under pressure. The rearrangement of the physical network may lead to the syneresis of oil. Hence, the response of the phantom to prolonged stress could be subject to future studies.

5. Conclusion

We have demonstrated that nanocellulose reinforcement increased the thermal stability of gelatin hydrogels and can be used to reinforce fat-mimicking phantoms for microwave application. Gelatin, CNC-gelatin, and DAC-gelatin reinforced emulsion all fulfill the requirements of phantom dielectric properties. Rheological measurements show that the CNC and DAC addition to the gelatin stabilized emulsion

abolish a clear gel-sol transition upon heating. The increased thermal stability of the CNC-gelatin and DAC-gelatin stabilized emulsions was confirmed by the QA test, where the gelatin reinforced phantom yielded under the stress and temperature of the antenna. The lower stress at break exhibited by the DAC-gelatin reinforced phantom made it more susceptible to mechanical failure during handling than the other two phantoms.

We have shown that a CNC-gelatin stabilized emulsion further transformed into CNC-gelatin reinforced phantom comply with the requirements for use as a fat tissue phantom for microwave diagnostics and hyperthermia treatment.

Acknowledgments

This work was financially supported by Wallenberg Wood Science Center (WWSC), VinnExcellence center ChaseOn, Barncancerfonden and Kristina Stenborg Stiftelse för Vetenskaplig Forskning. Chalmers Materials Analysis Laboratory is acknowledged for providing access to the CLSM.

Data availability statement

All data that support the findings of this study are included within the article (and any supplementary files).

ORCID iDs

Hana Dobšíček Trefná https://orcid.org/0000-0001-6025-0819
Anna Ström https://orcid.org/0000-0002-9743-1514

References

[1] Fhager A, Candefjord S, Elam M and Persson M 2018 Microwave diagnostics ahead: saving time and the lives of trauma and stroke patients *IEEE Microw Mag.* **19** 78–90
[2] Persson M *et al* 2014 Microwave-based stroke diagnosis making global prehospital thrombolytic treatment possible *IEEE Trans. Biomed. Eng.* **61** 2806–17
[3] Poplack S P *et al* 2007 Electromagnetic breast imaging: results of a pilot study in women with abnormal mammograms *Radiology* **243** 350–9
[4] Meaney P M *et al* 2013 Microwave imaging for neoadjuvant chemotherapy monitoring: initial clinical experience *Breast Cancer Res.* **15** 1–16
[5] Porter E, Coates M and Popović M 2015 An early clinical study of time-domain microwave radar for breast health monitoring *IEEE Trans. Biomed. Eng.* **63** 530–9
[6] Fear E C, Bourqui J, Curtis C, Mew D, Docktor B and Romano C 2013 Microwave breast imaging with a monostatic radar-based system: a study of application to patients *IEEE T Microw Theory.* **61** 2119–28
[7] Eadie L H 2016 Editorial: new technology and potential for telemedicine in battlefield brain injury diagnostics *Concussion.* **1**
[8] Datta N *et al* 2015 Local hyperthermia combined with radiotherapy and-/or chemotherapy: recent advances and promises for the future *Cancer Treat. Rev.* **41** 742–53
[9] Cihoric N *et al* 2015 Hyperthermia-related clinical trials on cancer treatment within the ClinicalTrials.gov registry *Int. J. Hyperthermia.* **31** 609–14
[10] Paulides M M, Dobsicek Trefna H, Curto S and Rodrigues D B 2020 Recent technological advancements in radiofrequency-andmicrowave-mediated hyperthermia for enhancing drug delivery *Adv. Drug. Deliv. Rev.* **163–164** 3–18
[11] Issels R D *et al* 2018 Effect of neoadjuvant chemotherapy plus regional hyperthermia on long-term outcomes among patients with localized high-risk soft tissue sarcoma: the EORTC 62961-ESHO 95 randomized clinical trial *JAMA Oncol.* **4** 483–92
[12] Joines W T, Zhang Y, Li C and Jirtle R L 1994 The measured electrical properties of normal and malignant human tissues from 50 to 900 MHz *Med. Phys.* **21** 547–50
[13] Martellosio A *et al* 2017 Dielectric properties characterization from 0.5 to 50 GHz of breast cancer tissues *IEEE Trans. Microwave Theory Tech.* **65** 998–1011
[14] Summers P E *et al* 2019 Towards mm-wave spectroscopy for dielectric characterization of breast surgical margins *The Breast.* **45** 64–9
[15] Lazebnik M *et al* 2007 A large-scale study of the ultrawideband microwave dielectric properties of normal breast tissue obtained from reduction surgeries *Phys. Med. Biol.* **52** 2637–56
[16] Lazebnik M *et al* 2007 A large-scale study of the ultrawideband microwave dielectric properties of normal, benign and malignant breast tissues obtained from cancer surgeries *Phys. Med. Biol.* **52** 6093–115
[17] Trefná H D *et al* 2017 Quality assurance guidelines for superficial hyperthermia clinical trials: II. Technical requirements for heating devices *Strahlenther Onkol.* **193** 351–66
[18] Dobšíček Trefná H *et al* 2019 Quality assurance guidelines for interstitial hyperthermia *Int. J. Hyperthermia.* **36** 276–93
[19] Hasgall P A *et al* (2018) IT'IS Database for thermal and electromagnetic parameters of biological tissues *Version 4.0* (https://doi.org/10.13099/VIP21000-04-0)
[20] Duan Q *et al* 2014 Characterization of a dielectric phantom for high-field magnetic resonance imaging applications *Med. Phys.* **41** 102303
[21] Ito K, Furuya K, Okano Y and Hamada L 2001 Development and characteristics of a biological tissue-equivalent phantom for microwaves *Electron. Commun. Jpn.* **84** 67–77
[22] Kato H and Ishida T 1987 Development of an agar phantom adaptable for simulation of various tissues in the range 5–40 MHz.(Hyperthermia treatment of cancer) *Phys. Med. Biol.* **32** 221
[23] Fontes-Candia C *et al* 2021 Maximizing the oil content in polysaccharide-based emulsion gels for the development of tissue mimicking phantoms *Carbohydr Polym.* **256** 117496
[24] Bini M G, Ignesti A, Millanta L, Olmi R, Rubino N and Vanni R 1984 The polyacrylamide as a phantom material for electromagnetic hyperthermia studies *IEEE Trans. Biomed. Eng.* **31** 317–22
[25] Kato H, Hiraoka M and Ishida T 1986 An agar phantom for hyperthermia *Med. Phys.* **13** 396–8
[26] Lazebnik M, Madsen E L, Frank G R and Hagness S C 2005 Tissue-mimicking phantom materials for narrowband and ultrawideband microwave applications *Phys. Med. Biol.* **50** 4245–58
[27] Madsen E L, Zagzebski J A and Frank G R 1982 Oil-in-gelatin dispersions for use as ultrasonically tissue-mimicking materials *Ultrasound Med. Biol.* **8** 277–87
[28] Yuan Y *et al* 2012 A heterogeneous human tissue mimicking phantom for RF heating and MRI thermal monitoring verification *Phys. Med. Biol.* **57** 2021–37
[29] Di Meo S *et al* 2019 Tissue-mimicking materials for breast phantoms up to 50 GHz *Phys. Med. Biol.* **64** 055006
[30] Di Meo S *et al* 2019 Tissue mimicking materials for breast phantoms using waste oil hardeners *13th European Conf. on*

Antennas and Propagation (EuCAP 2019) (Krakow, Poland, March 31-April 5)
[31] Allen S, Kantor G, Bassen H and Ruggera P 1988 Quality-assurance reports: CDRH RF phantom for hyperthermia systems evaluations *Int. J. Hyperthermia.* **4** 17–23
[32] Nikawa Y, Chino M and Kikuchi K 1996 Soft and dry phantom modeling material using silicone rubber with carbon fiber *IEEE T. Microw Theory* **44** 1949–53
[33] Garrett J and Fear E 2014 Stable and flexible materials to mimic the dielectric properties of human soft tissues *IEEE Antennas Wirel. Propag. Lett.* **13** 599–602
[34] Joachimowicz N, Conessa C, Henriksson T and Duchene B 2014 Breast phantoms for microwave imaging *IEEE Antennas Wirel. Propag. Lett.* **13** 1333–6
[35] Rydholm T, Fhager A, Persson M and Meaney P M 2017 A first evaluation of the realistic Supelec-breast phantom *IEEE J. Electromagn, RF, Microw. Med. Biol.* **1** 59–65
[36] Parker N G and Povey M J W 2012 Ultrasonic study of the gelation of gelatin: phase diagram, hysteresis and kinetics *Food Hydrocoll.* **26** 99–107
[37] Hellio D and Djabourov M 2006 Physically and chemically crosslinked gelatin gels *Macromol. Symp.* **241** 23–7
[38] van Vlierberghe S, Dubruel P and Schacht E 2011 Biopolymer-based hydrogels as scaffolds for tissue engineering applications: a review *Biomacromolecules.* **12** 1387–408
[39] Simon A, Grohens Y, Vandanjon L, Bourseau P, Balnois E and Levesque G 2003 A comparative study of the rheological and structural properties of gelatin gels of mammalian and fish origins *Macromol. Symp.* **203** 331–8
[40] Tosh S M and Marangoni A G 2004 Determination of the maximum gelation temperature in gelatin gels *Appl. Phys. Lett.* **84** 4242–4
[41] Djabourov M and Papon P 1983 Influence of thermal treatments on the structure and stability of gelatin gels *Polymer* **24** 537–42
[42] Dufresne A 2012 *Nanocellulose: From Nature to High Performance Tailored Materials.* (Munchen, Germany: Walter de Gruyter)
[43] Wang W, Zhang X, Teng A and Liu A 2017 Mechanical reinforcement of gelatin hydrogel with nanofiber cellulose as a function of percolation concentration *Int. J. Biol. Macromol.* **103** 226–33
[44] Mondragon G, Peña-Rodriguez C, González A, Eceiza A and Arbelaiz A 2015 Bionanocomposites based on gelatin matrix and nanocellulose *Eur. Polym. J.* **62** 1–9
[45] Kwak H W, Lee H, Park S, Lee M E and Jin H J 2020 Chemical and physical reinforcement of hydrophilic gelatin film with di-aldehyde nanocellulose *Int. J. Biol. Macromol.* **146** 332–42
[46] Dash R, Foston M and Ragauskas A J 2013 Improving the mechanical and thermal properties of gelatin hydrogels cross-linked by cellulose nanowhiskers *Carbohydr Polym.* **91** 638–45
[47] Takook P, Persson M, Gellermann J and Trefna H D 2017 Compact self-grounded Bow-Tie antenna design for an UWB phased-array hyperthermia applicator *Int. J. Hyperthermia.* **33** 387–400
[48] Trefna H D and Ström A 2019 Hydrogels as a water bolus during hyperthermia treatment *Phys. Med. Biol.* **64** 115025
[49] Sihvola A H 1999 *Electromagnetic Mixing Formulas And Applications.* (London, UK: The Institution of Electrical Engineers;)
[50] Markel V A 2016 Introduction to the Maxwell Garnett approximation: tutorial *J. Opt. Soc. Am. A. Opt. Image Sci. Vis.* **33** 1244–56
[51] Simpkin R 2010 Derivation of Lichtenecker's logarithmic mixture formula from maxwell's equations *IEEE T Microw Theory.* **58** 545–50
[52] Schuster E *et al* 2014 Microstructural, mechanical and mass transport properties of isotropic and capillary alginate gels *Soft Matter.* **10** 357–66